Russian Journal of Physical Chemistry, Vol. 79, No. 8, 2005, pp. 1279–1286. Translated from Zhurnal Fizicheskoi Khimii, Vol. 79, No. 8, 2005, pp. 1448–1456.

STRUCTURE OF MATTER AND QUANTUM CHEMISTRY

Molecular Dynamics of Hydrated Hydrocarbon Membrane Structures

E. V. Tourleigh*, K. V. Shaitan*, and N. K. Balabaev**

** Faculty of Biology, Moscow State University, Vorob'evy gory, Moscow, 119899 Russia*

*** Institute of Mathematical Problems of Biology, Russian Academy of Sciences, Pushchino, Moscow oblast, Russia*

E-mail: yegor@moldyn.org

Received July 26, 2004

Abstract—The distributions and transfer energies of several molecules and atomic groups between water and a structured hydrophobic phase were calculated by the molecular dynamics method. The coefficients of oxygen diffusion in a tetradecane membrane were estimated. The transfer energy of charged atomic groups was found to correlate with changes in the Born solvation energy. The contributions of atoms to the transfer energy of functional groups were shown to be nonadditive. The steered dynamics method for estimating the kinetic parameters of the penetration of molecules through interphase boundaries was developed.

INTRODUCTION

The molecular dynamics of heterogeneous and membrane structures is currently of considerable interest in view of the development of molecular technologies and biotechnologies. At the same time, the corresponding objects are fairly difficult for experimental studies [1, 2], and the basic laws of the dynamic behavior of such structures remain incompletely understood. This is also true of the microscopic picture of mass and energy transfer in strongly anisotropic structured heterogeneous media, the formation and relaxation of nonequilibrium supramolecular structures, and the special features of the distribution of molecular groups with different polarities at interphase boundaries. In this work, the molecular dynamics method involving the use of full-atomic force fields, special procedures, and fairly long trajectories is used to refine the microscopic picture of diffusion processes at the boundary between aqueous and membrane phases [3–5].

Extensive studies of the dynamics of biological membranes [6–9] and protein–membrane complexes raises the question of the optimization of computing procedures and modeling membrane structures by some hydrophobic medium [10]. There are comparatively simple models of a virtual hydrophobic medium [11]. The parameters of changes in the energy of groups in the transfer from water to a membrane are determined from the equilibrium constants in the water–octanol system in these models [10, 11]. The method of molecular dynamics allows the distribution functions of molecular groups in a water–membrane system to be calculated and possible nonadditive defects estimated.

Studies concerned with the diffusion of small molecules in membranes consisting of both biolipids and simpler organic compounds [12] usually fail to completely track the passive transmembrane transport of even very small molecules such as water, oxygen, ethanol, ammonia, and potassium and chlorine ions. A comparatively new approach is the steered molecular dynamics method [13] developed below. This method allows several complete transfers of the penetrating molecule under study through a membrane to be calculated with reasonable time expenditures.

In this work, we calculated the dynamics of several types of molecules, real and biologically important on the one hand and model (van der Waals spheres) on the other, for the example of a hydrated hydrocarbon membrane. Isothermal conditions were maintained using a collisional thermostat [14], which did not lead to nonlinear attractor modes distorting the statistically equilibrium distribution of energy over degrees of freedom [15].

EXPERIMENTAL

The PUMA package [16, 17] was specially modified to perform molecular dynamics calculations. The system of classical equations of motion of atoms was solved using the Amber99 force field [18].

We calculated membranes consisting of *n*-tetradecane $C_{14}H_{30}$ mono- and bilayers. The cell for calculations contained 24 tetradecane molecules per monolayer (Fig. 1a). Periodic boundary conditions were used. The initial structure corresponded to the perpendicular orientation of the axis of the largest extension of molecules with respect to the plane of the membrane. The hydrocarbon density in calculations at constant volume and temperature was of 0.707 to 0.771 g/cm^3 depending on the cell size (the experimental density of the volume phase is 0.761 g/cm^3 under normal conditions).

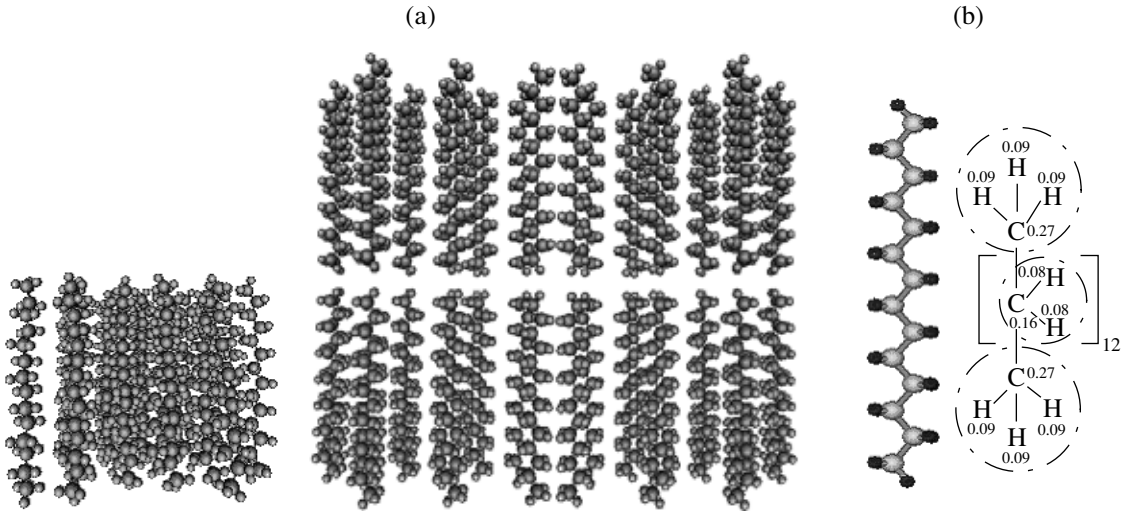

Fig. 1. (a) Tetradecane mono- and bilayer and (b) charge distribution in the tetradecane molecule (the CH_2 and CH_3 groups are taken to be electrically neutral).

The partial atomic charges in tetradecane were estimated according to Mulliken using the unrestricted Hartree–Fock method with the 6-31G* basis set. The charges accepted in our calculations are shown in Fig. 1b. An ordered membrane structure was formed using a parabolic potential that connected the tetradecane terminal carbon atom to a fixed plane. For the bilayer, there were two such planes situated in the middle of the bilayer at a distance of 4 Å from each other. We used the TIP3P model of water. The valence bonds and angles of water molecules were not fixed. In the starting configuration, water molecules were placed at a distance no less than 2.3 Å from the edge membrane atoms. The degree of solvation was determined as 15 water molecules per hydrocarbon molecule.

The cutoff radius of Coulomb interactions was 10 Å. Van der Waals interactions were cut off by means of multiplying Lennard-Jones potentials by the smoothing (switching) $W(r)$ function

$$W(r) = \begin{cases} 1, & r \le R_{on} \\ \dfrac{(R_{off}^2 - r^2)^2 (R_{off}^2 - 3R_{on}^2 + 2r^2)}{(R_{off}^2 - R_{on}^2)^3}, & \\ R_{on} < r < R_{off} & \\ 0, & r \ge R_{off}, \end{cases}$$

where r is the distance between the interacting atoms and the R_{on} and R_{off} parameters were set at 10 and 10.5 Å, respectively; the permittivity was assumed to be 1, and the step of integration was 1 fs.

The calculations were performed with periodic boundary conditions at a constant temperature. Both constant volume (*NVT* ensemble) and constant pressure (*NPT* ensemble) conditions were used. Constant pressure was maintained using a Berendsen barostat with the relaxation time of 100 ps equal in all three directions.

The temperature was varied from 300 to 1000 K. A constant temperature was maintained using a virtual collisional medium (collisional thermostat) [16, 17]. The mean frequency of collisions of virtual particles with atoms was 1 ps^{-1}, and the mass of virtual particles was 18 amu.

RESULTS AND DISCUSSION

At the first stage of calculations, the monolayer was allowed to relax for 200 ps (Fig. 2). The relaxation of the bilayer took nearly the same amount of time.

The hydrophobic properties of several small molecules were studied on the basis of their distribution between two phases, hydrophobic and aqueous.

We studied the dynamics of the diffusion of an oxygen molecule into the tetradecane bilayer. The simulations were performed in the *NVT* and *NPT* ensembles at 300 K. The starting position of the oxygen molecule was at the interphase boundary. The distribution of oxygen between two phases and the Gibbs energy of transfer from water to the bilayer at 300 K and external isotropic pressure 1 atm are shown in Fig. 3.

The free energy of oxygen transfer from water to the membrane at the given volumes of the aqueous and membrane phases was estimated as

$$\Delta F = \lim_{t\to\infty} \Delta F(t) = -kT \lim_{t\to\infty} \ln \frac{\int_{-a/2}^{+a/2} \rho(z,t)dz}{\int_{\varpi} \rho(z,t)dz},$$

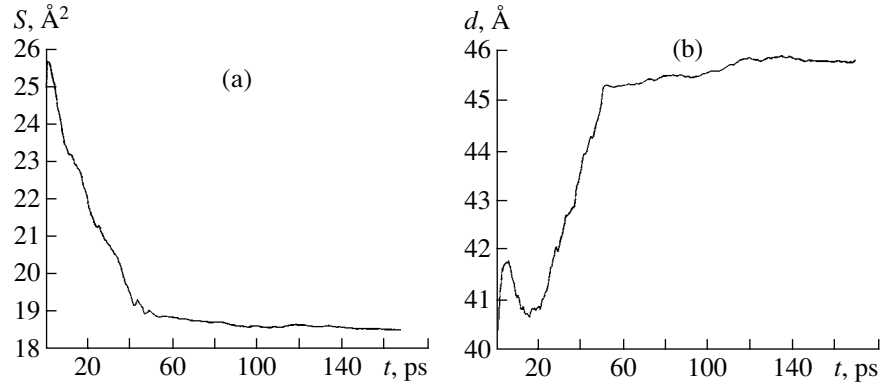

Fig. 2. Relaxation curves for (a) specific surface area and (b) cell thickness in a system with the tetradecane monolayer.

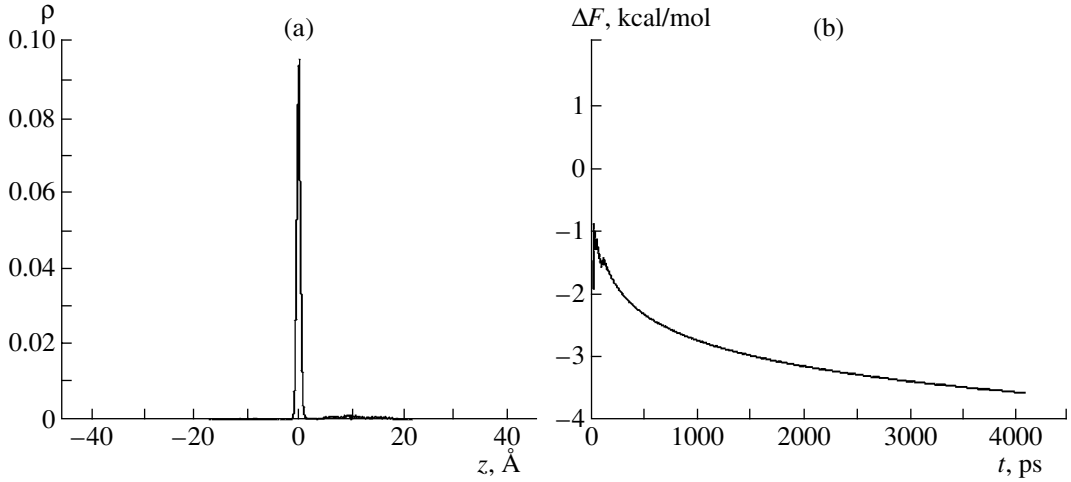

Fig. 3. (a) Oxygen molecule distribution between the bilayer and water and (b) Gibbs energy of oxygen transfer from water into the bilayer at 300 K and a constant isotropic pressure. See text for the notation.

where $\rho(z, t)$ is the probability density function of finding oxygen at a certain position along the z axis at the given time instant, $+a/2$ and $-a/2$ are the right and left bilayer boundaries, and the region of integration ω was $z > +a/2$ and $z < -a/2$. The free energy of oxygen transfer from water to the hydrophobic zone was more than 3.6 kcal/mol in magnitude; it was determined as a measure of the probability of oxygen molecule occurrence in the bilayer (including the boundary hydrophobic zone, about 3 Å thick) compared with the probability of its occurrence in water. The trajectory length in our numerical experiments was slightly larger than 4 ns. According to experimental estimates, the time of transmembrane oxygen diffusion in biological membranes is of 50 to 500 ns [19, 20].

Figure 3 shows that oxygen penetrates into the membrane in a comparatively short time (<50 ps) and remains there during most of the time of computations; it is predominantly localized in the center of the bilayer, where the largest free volume is. A similar effect was observed in biomembranes in experiments with spin labels [21–23].

The one-dimensional oxygen diffusion coefficient in the direction normal to the membrane, two-dimensional diffusion coefficient in the plane of the bilayer, and three-dimensional diffusion coefficient were calculated as the coefficients of the linear approximations of the curves

$$\langle z(t)^2 \rangle = 2D_z t,$$

$$\langle x(t)^2 + y(t)^2 \rangle = 4D_{xy} t,$$

$$\langle x(t)^2 + y(t)^2 + z(t)^2 \rangle = 6D_{xyz} t,$$

respectively. The angle brackets denote averaging over the whole trajectory. The oxygen diffusion coefficients (cm^2/s) in the bilayer–water system at 300 K and 1 atm are $D_z = 1.71 \times 10^{-5}$, $D_{xy} = 3.09 \times 10^{-5}$, and $D_{xyz} = 2.63 \times 10^{-5}$ for the bilayer and 4.73×10^{-5} for water.

The oxygen diffusion coefficients obtained are in agreement with the known experimental estimates for the diffusion of oxygen in biological membranes, which range from 1.5×10^{-5} to 4.7×10^{-5} cm^2/s [19, 20,

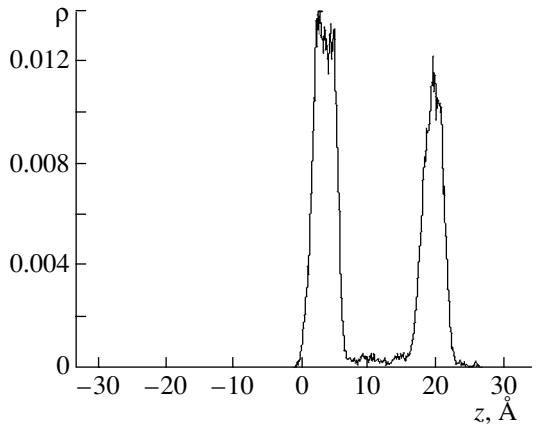

Fig. 4. Oxygen molecule distribution between the bilayer and water at 300 K and a constant volume; the trajectory length is 6 ns.

24]. These data are also in agreement with the diffusion coefficients obtained in molecular dynamics calculations (for instance, with the diffusion coefficient in the hexadecane monolayer, 2.6×10^{-5} cm^2/s according to [25]). The calculated oxygen diffusion coefficients in water are more than two times larger than the experimental values for volume diffusion (from 1.76×10^{-5} to 2.3×10^{-5} cm^2/s at 300 K [26–28]). These results are in agreement with the data reported in [29], according to which the self-diffusion coefficient of TIP3P water is also overestimated compared with the experimental value by a factor of more than two. The Stokes–Einstein formula

$$D = k_B T/6\pi\eta r$$

for the diffusion coefficient of oxygen (η is the viscosity of the solvent and r is the radius of the molecule) yields a viscosity of tetradecane in the volume phase of 2.0–2.6 cP [30], which is close to the calculated values.

The distribution of oxygen between the two phases at a constant volume is somewhat different (Fig. 4). The constant volume condition and a comparatively small calculation cell size restrict density fluctuations in both phases. Oxygen then occurs on the surface of the hydrophobic layer during most of the time.

Table 1. Main types of atoms of the Amber force field

Atom type	Charge, e	r_{VDW}, Å	ε, kcal/mol
C_{aliph}	−0.0463	1.9080	0.1094
C_{arom}	0.2924	1.9080	0.0860
C_{hetero}	0.5382	1.9080	0.0860
N	−0.4698	1.8240	0.1700
O	−0.3180	1.7210	0.2104
O*	−0.6137	1.6612	0.2100
S	−0.2525	2.0000	0.2500

We also estimated the influence of the charge of a molecule on its distribution between two phases, the tetradecane monolayer and water. We calculated the dynamics of seven types of atoms with partial charges that corresponded to the main types of nonhydrogen atoms of the Amber force field (Table 1). Such calculations may prove helpful in the development of continual hydrophobic medium models. For instance, interactions with a membrane were modeled in [10] by changes in the potential energy of atoms caused by transfer from the aqueous to hydrophobic phase. These changes were calculated from the transfer energies of amino acids from water to octanol [31]. No complete agreement of the experimental data with the scale of hydrophobicity of amino acids was, however, obtained. According to [11], not only the hydrophobic characteristics of atoms but also the fraction of the surface of atomic spheres exposed to the membrane and aqueous media should be included. We use a simpler model, in which the hydrophobic characteristics of typical force field atoms are calculated from the distribution functions of atoms in the membrane–water system.

We studied the distributions of atomic particles with Amber force field parameters in the membrane–water system. The charge of atoms of every type was determined by averaging over all possible charges that it had in amino acids taking into account their frequencies of occurrence in proteins [32].

Table 1 contains the effective charges of atoms, their van der Waals radii, and the energy parameters of van der Waals interactions. Trajectories 5 to 7 ns long were calculated. The calculations were performed for the *NVT* ensemble at 1000 K to accelerate the procedure of configuration space scanning.

The distributions of the most hydrophobic and most hydrophilic ions are shown in Fig. 5 (the upper and lower rows, respectively). As expected, the ions with lower charges were more hydrophobic.

Note that the ratio between the charge z and hydrophobic properties of an ion can be estimated from the Born theory, which also takes into account the ion size r. According to this theory, the change in the electrostatic component of the Gibbs energy caused by the transfer of an ion from water into a membrane layer can be estimated as

$$\Delta W_B = \frac{z^2 e^2}{8\pi r \varepsilon_0}\left(\frac{1}{\varepsilon_2} - \frac{1}{\varepsilon_1}\right),$$

where ε_1 and ε_2 are the relative permittivities of water and the nonpolar solvent ($\varepsilon_1 \approx 80$ and $\varepsilon_2 \approx 2$–3).

The calculated free energies of transfer of atoms from water into the monolayer correlate with changes in the Born energy (Fig. 6). Ions with lower charges and larger diameters are more strongly stabilized in the membrane. These results are in agreement with the experimental data on the penetration of ions through

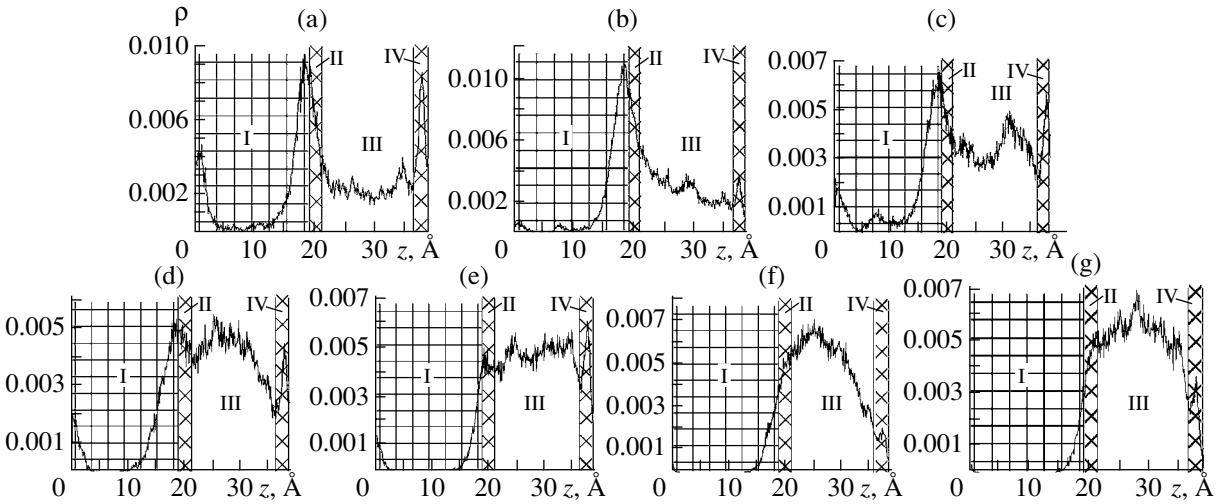

Fig. 5. Distribution profiles for the atoms (a) C_{aliph}, (b) S, (c) C_{arom}, (d) O, (e) N, (f) O*, and (g) C_{hetero}. Order of zones: (I) hydrocarbon monolayer, (II) surface hydrophobic layer, (III) aqueous layer, and (IV) surface hydrophobic layer (on the opposite side of the hydrocarbon monolayer).

the water–oil interphase boundary, which correlate well with Born solvation energies [33].

Special calculations showed that the contributions of separate atoms to the distribution of functional groups were not additive (cf. Figs. 5 and 7). For instance, the distribution of the CO group was not the sum of the distributions of C_{hetero} and O*, which constitute the CO group. For CO, the likely reason for this is the appearance of a dipole moment when the group is formed. It follows that the possibility of using a simple model based on the introduction of some specific hydrophobic characteristic for every type of atom proves to be very problematic.

We also considered the distributions between water and the hydrocarbon phase of six amino acid residues with different polarities (Ala, Asp, Gly, Phe, Trp, and Val) at 300 K. The cell with the hydrated tetradecane monolayer was then maintained at a constant pressure of 1 atm. The specific surface area per tetradecane molecule was 18.2 Å^2. The starting position of the amino acids was at the monolayer boundary. The plots of the distribution of the residues are given in Fig. 8. None of the residues succeeded in penetrating into the monolayer during 10 ns of computations. This shows that, at the given membrane density, the interphase boundary is a serious obstacle to the penetration of amino acid residues.

The energy of amino acid transfer from water to octanol [30] is frequently used as a measure of the hydrophobic properties of the corresponding residues. Applying this criterion, we find that the most hydrophobic amino acid residues concentrate at the tetradecane boundary, whereas more hydrophilic residues reside in the aqueous phase during a somewhat longer time.

The calculations described above were performed under equilibrium conditions. At the same time, nonequilibrium dynamics methods are currently being developed to handle nonequilibrium systems. We also

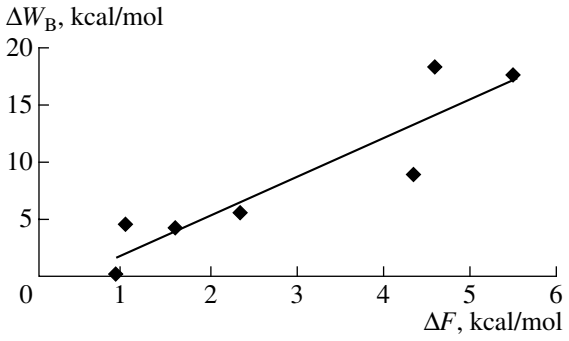

Fig. 6. Correlation between the calculated energy of transfer and the corresponding Born energy for seven types of atoms; correlation coefficient 0.9167.

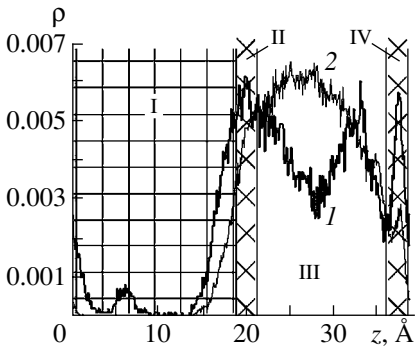

Fig. 7. (*1*) CO group distribution profile and (*2*) the sum of distribution profiles for the C_{hetero} and O atoms; trajectory length 5 ns. See Fig. 5 for zone denotations (I–IV).

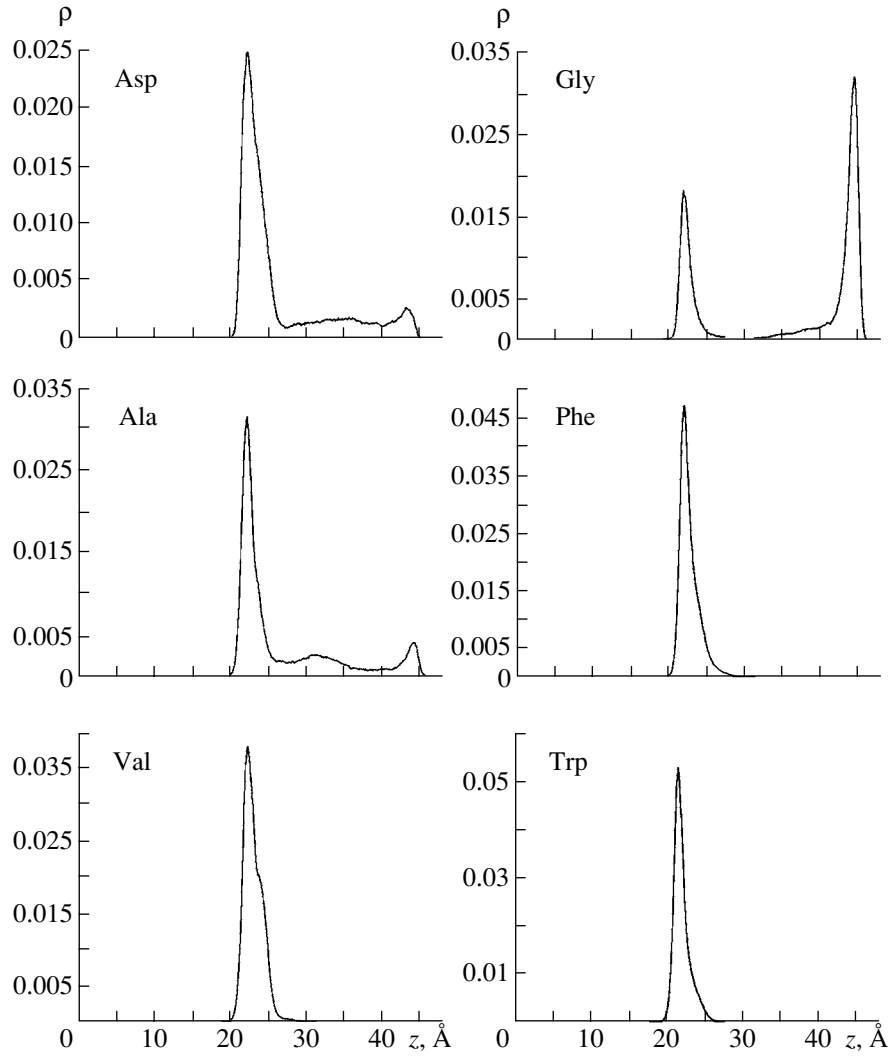

Fig. 8. Distribution density of an amino acid residue along the normal to the membrane z averaged over atoms (averaging is performed with weight factors proportional to atomic weights). The order in which the plots are arranged (from left to right and from top to bottom) corresponds to decreasing the Gibbs energy of amino acid transfer from water to octanol. Monolayer boundaries along the z axis are $z = 0$ and 20 Å (taking into account periodic boundary conditions, $z = 46$ Å is also a monolayer boundary); the aqueous phase occupies space between 20 and 46 Å.

developed an approach to the dynamics of membrane structure that uses nonequilibrium steered dynamics methods. Additional external forces (constant or varying with time) then act on separate atoms.

We studied the dynamics of model spheres that interacted with the other atoms only by van der Waals forces. The force applied to a probe particle was a sine function of time and was directed normally to the membrane. The mean force value was set at 1 to 10 kcal/(Å mol) (1 kcal/(Å mol) ≈ 70 pN).

Our numerical experiment showed that spheres of radii 2 and 4 Å moved in the TIP3P aqueous medium at velocities of 10 and 2.6 Å/ps, respectively, at a constant external force of 10 kcal/(Å mol). That is, the Stokes law was likely violated slightly at particle radii smaller than or close to the radius of medium molecules. When a particle of radius 2 Å moves, the effective viscosity of the medium is approximately two times lower than for large particles.

We studied the penetration of particles under the action of an external force through the membrane layer. Probe spheres penetrated through the layer in time of about 2.5 ns under the action of a force whose mean value was no less than 7 kcal/(Å mol) (Table 2).

A substantial decrease in the time of repeat penetrations shows that pore formation plays a decisive role in penetration through the tetradecane monolayer. Forcing a sphere through a monolayer results in the formation of a pore and deformation of the surrounding membrane structure. The relaxation time of such a pore is comparatively long. For instance, after a series of many particle passages under the action of a constant force of

10 kcal/(Å mol) (Table 2), the last passage took time as short as 9 ps. Shifting the probe sphere in the plane of the membrane by a distance equal to its radius increased the passage time to 12 ps; for a distance equal to the diameter, the time of passage increased a bit, to 20 ps.

The forced transport of a probe molecule in a medium at the parameter values under consideration does not depend linearly on the force applied. We also did not observe resonance effects over the range of external force frequency variations that we studied.

A comparison of the directed movement of a sphere of radius 4 Å and the alanine residue of effective radius 3.1 Å (Table 3) through a layer of tetradecane shows that increasing the force is not accompanied by a proportional increase in the rate of repeat alanine passages through the membrane. For the sphere, an increase in the rate is essentially nonlinear. Note that, unlike a sphere, the alanine residue is flexible to a certain degree. It appears that the degree of membrane deformation and activation barrier values related to pore formation are quite different for spheres and alanine residues.

To summarize, the simplest full-atomic model of a hydrated membrane structure used in this work allows us to study the laws that govern the distribution of various molecules between two phases, hydrophobic structured and aqueous. We showed that only very small and strongly hydrophobic molecules, for instance, oxygen, can penetrate on their own into a membrane layer under normal conditions in times shorter than 10 ns. At a fixed volume, penetration into a structured membrane medium is strongly impeded. We observed oxygen accumulation in the middle of the bilayer, which was caused by increased looseness of the structure at the interface between two monolayers.

A study of the dynamics of spontaneous transmembrane diffusion in times on order of 10 ns requires calculations at elevated temperatures. The free energy of transfer calculated at 1000 K for the main types of Amber99 atoms varies from 0.9 to 5.5 kcal/mol. These energy changes well correlate with changes in the corresponding Born solvation energies. The Helmholtz energy of transfer increases (that is, hydrophobic properties weaken) in the series of atoms C_{aliph}, S, C_{arom}, O, N, O*, C_{hetero}. Importantly, atomic contributions to the free energy of transfer of functional groups are not additive. This impedes the continual simulation of hydrophobic media by including an additional term describing the interaction of atoms with this medium into the potential energy.

The calculated distributions of amino acid residues between phases are in conformity with their known hydrophobic properties. Note that, under the specified conditions of calculations, a membrane is a very substantial barrier to the penetration of amino acid residues into it.

Table 2. Characteristic times of passage through the membrane under the action of a periodic force $F(t) = \bar{F}_0 + C_0\sin(2\pi t/T)$, where C_0 = 2 kcal/Å/mol, for $\bar{F}_0$ = 7 and 10 kcal/Å/mol; at $T = \infty$, $F(t) = \bar{F}_0$ = const; particle radius 4 Å

$\bar{F}_0$, kcal/(Å mol)	T, ps	τ_1, ps	$\bar{\tau}$, ps	$\bar{\tau}_2$, ps
7	0.1	>2500 ps	–	–
7	1	1268	214	108
7	∞	724	149	101
10	0.1	155	15	13
10	1	1547	48	15
10	∞	1899	173	29

Note: $\bar{F}_0$ is the mean external force, T is the period, τ_1 is the time of the first passage, $\bar{\tau}$ is the mean time of all passages, and $\bar{\tau}_2$ is the mean time of all except the first passages.

Table 3. Time of passage of molecules of various diameters through the membrane under the action of a constant force (F_0)

F_0, kcal/(Å mol)	R_0, Å	τ_1, ps	$\bar{\tau}$, ps	τ_2, ps
7	3.1	660	25	16
7	4	724	149	101
10	3.1	21	18	15
10	4	1899	173	29

Note: R_0 is the effective radius of the molecule; see Table 2 for the other notation.

A consideration of equilibrium dynamics processes of even comparatively small molecules in such a system does not allow us to draw final conclusions on the balance of hydrophobic forces at room temperature at the expense of reasonable computing time expenditures. The steered dynamics method that we are developing can be used to organize a directed and faster scenario of the development of events for certain degrees of freedom. The kinetic coefficients calculated this way are related to the equilibrium parameters of the system by thermodynamic and statistical equations. The degree to which the system is nonequilibrium should then, however, be controlled. For instance, nonlinear dependences of the velocities of directed molecule movements on the external force value appear already at velocities of 10^5 cm/s. Special studies of the reasons for this effect (weakly nonequilibrium state of the system and (or) the non-Newtonian character of the medium) are beyond the scope of this work. The same is true of the dynamics of formation and relaxation of supramolecular membrane structures (pores in the context of this work). The formation of a pore dramatically changes the dynamics of transmembrane transport. The relaxation time of a pore in the membrane under study is comparatively long (more than 10 ps), and memory

effects in the dynamics of membranes can be very significant.

ACKNOWLEDGMENTS

This work was in part financially supported by the Ministry of Science of the Russian Federation, Russian Foundation for Basic Research (project no. 04-04-49645), and Ministry of Education of the Russian Federation ("Integration" program, project no. I0431).

REFERENCES

1. R. S. Armen, O. D. Uitto, and S. E. Feller, Biophys. J. **75**, 734(1998).
2. H. Bürsing, S. Kundu, and P. Vöhringer, J. Phys. Chem. B **107**, 2404 (2003).
3. H. Heller, M. Schaefer, and K. Schulten, J. Phys. Chem. **97**, 8343 (1993).
4. K. V. Shaitan and P. P. Pustoshilov, Biofizika **44** (3), 436 (1999) [Biophysics **44** (3), 429 (1999)].
5. N. K. Balabaev, A. L. Rabinovich, P. O. Ripatti, and V. V. Kornilov, Zh. Fiz. Khim. **72** (4), 686 (1998) [Russ. J. Phys. Chem. **72** (4), 595 (1998)].
6. A. L. Rabinovich, P. O. Ripatti, and N. K. Balabaev, J. Biol. Phys. **25**, 245 (1999).
7. A. L. Rabinovich, P. O. Ripatti, N. K. Balabaev, and F. A. M. Leermakers, Phys. Rev. E: Stat. Phys., Plasmas, Fluids, Relat. Interdiscip. Top. **67**, 011909.
8. F. A. M. Leermakers, A. L. Rabinovich, and N. K. Balabaev, Phys. Rev. E: Stat. Phys., Plasmas, Fluids, Relat. Interdiscip. Top. **67**, 011910.
9. A. L. Rabinovich, P. O. Ripatti, and N. K. Balabaev, Zh. Fiz. Khim. **76** (11), 2007 (2002) [Russ. J. Phys. Chem. **76** (11), 1814 (2002)].
10. O. Edholm and F. Jähnig, Biophys. Chem. **30**, 279 (1998).
11. R. Efremov, P. Volynsky, D. Nolde, *et al.*, Theor. Chem. Acc. **106**, 48 (2001).
12. D. P. Tieleman, S. J. Marrink, and H. J. C. Berendsen, Biochim. Biophys. Acta **1331**, 235 (1997).
13. S. Park and K. Schulten, J. Chem. Phys. **120**, 5946 (2004).
14. K. V. Shaitan and S. S. Saraikin, Zh. Fiz. Khim. **76** (6), 1091 (2002) [Russ. J. Phys. Chem. **76** (6), 987 (2002)].
15. V. L. Golo and K. V. Shaitan, Biofizika **47** (4), 611 (2002) [Biophysics **47** (4), 567 (2002)].
16. A. S. Lemak and N. K. Balabaev, Mol. Simul. **15**, 223 (1995).
17. A. S. Lemak and N. K. Balabaev, J. Comput. Chem. **17**, 1685 (1996).
18. J. Wang, Cieplak, and P. A. Kollman, J. Comput. Chem. **21**, 1049 (2000).
19. A. Lavi, Biophys. J. **82**, 2101 (2002).
20. M. Roslaniec, J. Photochem. Photobiol., B **57**, 149 (2000).
21. A. Ligeza, A. N. Tikhonov, J. S. Hyde, and W. K. Subczynski, Biochim. Biophys. Acta **1365** (3), 453(1998).
22. D. Marsh, Proc. Natl. Acad. Sci. USA **98** (14), 7777 (2001).
23. B. G. Dzikovski, V. A. Livshits, and D. Marsh, Biophys. J. **385**, 1005 (2000).
24. M. V. Merx, FASEB J. **15**, 1077 (2001).
25. S. J. McKinnon, S. L. Whittenburg, and B. Brooks, J. Phys. Chem. **96**, 10497 (1992).
26. S. Th. Bouwer, L. Hoofd, and F. Kreuzer, Biochim. Biophys. Acta **1338**, 127 (1997).
27. T. Itoh, K. Yaegashi, T. Kosaka, and H. Fukushima, Biorheology **33** (1), 80 (1996).
28. C. E. St-Denis and C. J. Fell, Can. J. Chem. Eng. **49**, 885 (1971).
29. M. W. Mahoney and W. L. Jorgensen, J. Chem. Phys. **114**, 363 (2001).
30. H. S. Park, T. Chang, and S. H. Lee, J. Chem. Phys. **113**, 5502 (2000).
31. J. L. Fauchère and V. Pliska, Eur. J. Med. Chem. **18**, 369 (1986).
32. G. E. Schulz and R. H. Schirmer, *Principles of Protein Structure* (Springer, New York, 1979; Mir, Moscow, 1982).
33. K. Wu, M. J. Iedema, and J. P. Cowin, Science (Washington, D.C.) **286**, 2482 (1999).